M-ary-state phase-shift-keying discrimination below the homodyne limit

F. E. Becerra,[1,*] J. Fan,[1] G. Baumgartner,[2] S. V. Polyakov,[1] J. Goldhar,[3] J. T. Kosloski,[4] and A. Migdall[1]

[1]*Joint Quantum Institute, Department of Physics, University of Maryland, and National Institute of Standards and Technology, 100 Bureau Drive, Gaithersburg, Maryland 20899, USA*

[2]*Laboratory for Telecommunications Sciences, 8080 Greenmead Drive, College Park, Maryland 20740, USA*

[3]*Department of Electrical and Computer Engineering, 2410 A.V. Williams Building, University of Maryland, College Park, Maryland 20742, USA*

[4]*Department of Electrical and Computer Engineering, Johns Hopkins University, Baltimore, Maryland 21218, USA*

(Received 1 September 2011; published 22 December 2011)

We investigate a strategy for *M*-ary discrimination of nonorthogonal phase states with error rates below the homodyne limit. This strategy uses feed forward to update a reference field and signal nulling for the state discrimination. We experimentally analyze the receiver performance using postprocessing and a Bayesian strategy to emulate the feed-forward process. This analysis shows that for a moderate system detection efficiency, it is possible to surpass the homodyne error limit for quadrature phase-shift keying signals using feed forward.

DOI: 10.1103/PhysRevA.84.062324 PACS number(s): 03.67.Hk, 03.65.Ta, 42.50.Ex

I. INTRODUCTION

Perfect discrimination of nonorthogonal quantum states is impossible; there is no physical measurement that allows the discrimination of such states with total certainty [1]. Quantum cryptography in the form of quantum key distribution (QKD) uses nonorthogonal states to guarantee secure communication between the transmitter and the receiver through the creation and sharing of a secret key [2]. For QKD using coherent states, the key rate is limited by the performance of the state discrimination of the receiver [3]. This is because errors caused by the receiver have a similar signature to the loss of information due to an eavesdropper. Even in the case of classical communications where amplification is not possible (such as a free-space link), the nonorthogonality of coherent states produces unwanted errors in decoding the information [1,4,5]. This has led to significant efforts to find and demonstrate measurement strategies for optimal discrimination of nonorthogonal states approaching the limits set by quantum mechanics [1], and thus to increase the capacity of the communication channels [6], thereby reducing the demand on resources [1,4,5,7,8].

In binary optical communication the transmitter encodes one bit of information per optical information carrier. However, in *M*-ary communication, the optical carrier contains more than one bit of information, increasing the channel capacity and reducing the resources required. When the information is encoded in coherent states, the minimum probability of error for conventional receivers is referred to as the homodyne limit (HL) and is due to the inherent overlap of the states involved. However, quantum mechanics allows lower error probabilities for the discrimination of such nonorthogonal states. The Helstrom bound is the ultimate limit for the case of two nonorthogonal states (binary signals), and also for multiple nonorthogonal states such as quadrature phase-shift keying (QPSK) [1].

Optimized strategies for binary signal receivers using photocounting and displacement of the signal state to the vacuum state, using a local oscillator (LO) field, have shown theoretical error probabilities below the HL [9–12]. Proof-of-principle experiments have tested some of these strategies for on-off-keying [13] and binary-phase-shift-keying [14] signals. Recently, optimized-displacement receivers, where the LO parameters are set for minimum error probability, have been realized surpassing the HL for on-off-keying [15] and binary-phase-shift-keying [16] signals.

In the case of *M*-ary communication, proposals for optimized strategies using feedback and feed forward have shown theoretical error probabilities below the HL for QPSK signals. One feedback receiver for QPSK [7] updates the LO phase to displace the signal to vacuum by destructive interference (signal nulling). Another feed-forward receiver scheme for QPSK [8] is a hybrid system consisting of a homodyne receiver and a subsequent optimized displacement receiver using feed forward. However, there is no strategy for general *M*-ary-state discrimination with error rates below the homodyne limit, and no experimental investigation of a receiver for QPSK with a strategy with error probabilities below the HL has been reported. Therefore the feasibility of any practical implementation of receivers for *M*-ary signals is yet to be determined.

In this article we describe a strategy for *M*-ary-phase-state discrimination below the HL using feed forward and signal nulling. We test this strategy experimentally for a QPSK receiver using postprocessing to emulate the feed-forward process and multiple discrimination stages applying signal nulling. This analysis shows that a receiver with moderate system detection efficiencies (DEs) and a small number of stages would be sufficient for QPSK-state discrimination below the HL.

Section II describes the strategy for *M*-ary-state discrimination; we describe the experimental realization of the QPSK receiver using postprocessing in Sec. III; Sec. IV contains the analysis of the experimental data and the results; and we give our concluding remarks in Sec. V.

II. *M*-ARY-STATE DISCRIMINATION STRATEGY

M-ary phase-encoded communication encodes the information in the phase of a coherent state, and the receiver

*fbecerra@umd.edu

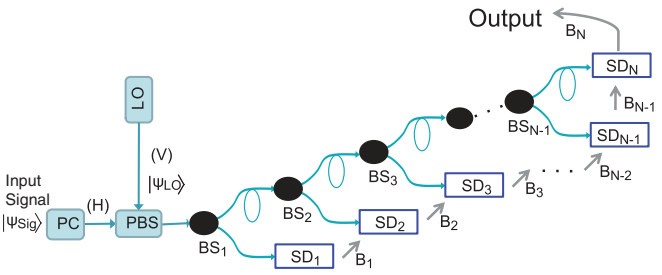

FIG. 1. (Color online) Feed-forward state-discriminating receiver. The polarization of the signal is set by the polarization controller (PC). After the polarizing beam splitter (PBS), the signal (with horizontal polarization) and LO (with vertical polarization) propagate together and are distributed to each state-discriminating stage (SD_n) through a series of beam splitters (BSs). Inside each SD stage the signal interferes with a fraction of the local oscillator, which has been projected or rotated onto the signal polarization, to test a particular signal state. Alternatively, this receiver can be implemented using a $1 \times N$ splitter after the PBS, and performing adaptive measurements in the N outputs in a feed-forward manner.

discriminates among the M possible states of the signal using a LO as a phase reference. The receiver investigated here uses multiple signal-nulling stages and feed forward to update the relative phase of the signal and LO in subsequent stages. The updated phase setting in a given stage is based on the results of the previous ones (measurement history), so that the LO tests the current most likely hypothesis of the signal. We describe this strategy for M-ary phase-encoded state discrimination and a design for its experimental implementation.

Our proposed M-ary phase-shift receiver architecture (Fig. 1) has significant advantages when considering implementations with current technology, making it possible to approach optimal receiver performance and exceed the sensitivity of an ideal homodyne receiver. The receiver distributes the signal and LO (which are orthogonally polarized) among the state discrimination (SD) stages. The copropagation of the signal and LO reduces the need to stabilize separate optical paths in each stage, lowering complexity and making it feasible to implement a larger number of stages to achieve higher sensitivities (see discussion below).

The M-ary phase-shift-keying (PSK) signal enters the receiver in a coherent state $|\psi_{\rm Sig}\rangle = |e^{i\phi_{\rm Sig,M}}\sqrt{n_{\rm Sig}}\rangle$ with horizontal polarization (H), an average photon number $n_{\rm Sig}$, and a phase $\phi_{\rm Sig,M} = \frac{2\pi s}{M}$ representing one of the $s \in [1,\ldots,m,\ldots,M] = \mathbb{M}$ symbols of the alphabet with *a priori* probabilities $\mathbb{B}_0 = \{\zeta_0(1),\ldots,\zeta_0(m),\ldots,\zeta_0(M)\}$. The task of the receiver is to identify the symbol s with the minimum probability of error. While equal *a priori* probabilities, $\zeta_0(m) = \frac{1}{M}$, for all the possible symbols $m \in \mathbb{M}$ of the input signal s are typical for communication systems, it is not required for the operation of our receiver. The signal state $|\psi_{\rm Sig}\rangle$ can be represented by the Jones vector defined in the (H,V) basis:

$$|\psi_{\rm s}\rangle = \begin{bmatrix} e^{i\phi_{\rm Sig,M}}\sqrt{n_{\rm Sig}} \\ 0 \end{bmatrix}.$$

At the polarizing beam splitter (PBS), the signal combines with a strong coherent LO $|\psi_{\rm LO}\rangle = |e^{i\pi}\sqrt{n_{\rm LO}}\rangle$, with average LO photon number $n_{\rm LO}$ ($n_{\rm LO} \gg n_{\rm Sig}$) and vertical polarization (V). The Jones vector describing the LO is given by

$$|\psi_{\rm LO}\rangle = \begin{bmatrix} 0 \\ e^{i\pi}\sqrt{n_{\rm LO}} \end{bmatrix}.$$

The copropagating signal and LO are distributed to the various stages using the branched beam splitters (BSs). (Compensation of polarization mode dispersion can be used to ensure temporal overlap and orthogonality of the signal and LO if necessary.) While the beam splitter reflectivities should be chosen to uniformly distribute the signal energy to each of the receiver's stages, absolute optimization only marginally improves receiver performance for $M > 2$ compared with the near optimal case of uniform signal distribution.

The state of the total field entering each SD stage of a receiver with N discrimination stages is

$$|\psi_{\rm Sig,LO}(\phi)\rangle = \frac{1}{\sqrt{N}}\begin{bmatrix} e^{i\phi_{\rm Sig,M}}\sqrt{n_{\rm Sig}} \\ e^{i\pi}\sqrt{n_{\rm LO}} \end{bmatrix}, \quad (1)$$

where the global phase acquired by the state has been omitted without loss of generality, since only the relative phase between the signal and LO affects the receiver performance. The receiver uses interferometric measurements in each stage to test the hypothesis of the signal phase relative to the LO. A polarizer mixes the incident signal entering the stage with a small fraction of the strong LO with a given phase producing interference, and a single-photon detector (SPD) measures this interference.

At SD_1 the phase of the LO, δ_{h_1}, is set based on the signal hypothesis h_1 using a Pockels cell on the combined signal and LO beam. The Pockels cell, modulating just one polarization, allows the relative signal-LO phase $\phi_{\rm Sig,M} - \delta_{h_1} + \pi$ to be controlled, ideally producing a null detection via destructive interference (signal nulling). The state of the total field after the Pockels cell is now

$$|\psi_{\rm Sig,LO}(\phi,\delta)\rangle = \frac{1}{\sqrt{N}}\begin{bmatrix} e^{i\phi_{\rm Sig,M}}\sqrt{n_{\rm Sig}} \\ -e^{i\delta_{h_1}}\sqrt{n_{\rm LO}} \end{bmatrix}. \quad (2)$$

The signal and LO pass through a polarizer oriented at angle χ_1 relative to the horizontal to combine a fraction $T_1 = \cos^2(\chi_1)$ of the signal field with the fraction $1 - T_1 = \sin^2(\chi_1)$ of the LO field, where $T_1 \approx 1$. This has the effect of interfering a large fraction of the signal with a small fraction of the LO [see Fig. 2(a)]. The amplitude of the optical state after the polarizer is

$$\langle\vec{p}|\psi_{\rm Sig,LO}(\phi,\delta_1)\rangle = \frac{1}{\sqrt{N}}(\sqrt{n_{\rm Sig}}\sqrt{T_1}e^{i\phi_{\rm Sig,M}} - \sqrt{n_{\rm LO}}\sqrt{1-T_1}e^{i\delta_{h1}}), \quad (3)$$

where $\vec{p} = [\frac{\sqrt{T_1}}{\sqrt{1-T_1}}]$ is the projection due to the polarizer. Alternatively, the receiver can use different paths for the signal and LO instead of polarization modes in each stage to reduce possible losses of the signal due to absorption in the Pockel cells. Figure 2(b) shows an interferometer using different optical paths where a PBS separates the signal and LO within

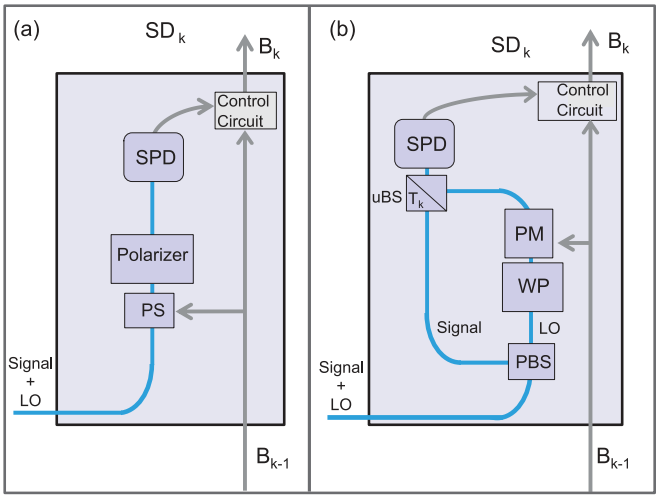

FIG. 2. (Color online) (a) SD stage using a Pockels cell as a phase shifter (PS) and a polarizer oriented at angle χ to combine fractions of the signal and LO to achieve interference at a single-photon detector (SPD). (b) Alternative SD-stage design using separate paths for the signal and LO instead of polarization modes. The signal and local oscillator separate at a PBS, with the LO passing through a wave plate (WP) and a phase modulator (PM). The wave plate rotates the polarization of the LO to match the signal so that they interfere at the unbalanced beam splitter (uBS) with transmissivity T_k for the signal in the stage k. The control circuit uses the detection results to calculate the new probabilities of the states and passes them to the next stage.

the stage. A wave plate (WP) rotates the polarization of the LO to match the signal and a phase modulator (PM) adjusts the LO phase preparing the stage to test hypothesis h_k. The signal and LO interfere at the unbalanced beam splitter with transmissivity $T_k \approx 1$ for the signal path. The mean photon number of the total field at the detector of stage k is

$$\langle n_k(s,h_k)\rangle = \frac{1}{N}\big\{n_{\rm Sig}T_k + n_{\rm LO}(1-T_k) - 2\sqrt{n_{\rm Sig}n_{\rm LO}(1-T_k)(T_k)}\cos(\phi_{\rm Sig,M}-\delta_{h_k})\big\}. \quad (4)$$

When the hypothesis of the signal state is correct (i.e., $\delta_{h_1} = \phi_{\rm Sig,M}$), it is necessary to have equal signal and LO intensities at the detector to yield a null detection. To achieve this balance we set the transmissivity to $T_k = \frac{n_{\rm LO}}{n_{\rm Sig}+n_{\rm LO}}$, and the mean photon number of the total field at the detector becomes

$$\langle n_k(s,h_k)\rangle = n_{\rm Sig}\frac{2T_k}{N}\big[1-\cos\big(\phi_{\rm Sig,M}-\delta_{h_k}\big)\big].$$

We note that the condition $T_k \approx 1$ ($\chi \ll 1$) follows from $n_{\rm LO} \gg n_{\rm Sig}$ (remembering that these photon numbers are defined at the input of the receiver).

The phase hypothesis and detection result together provide information about the phase of the incident signal, which is used for the subsequent measurements. Based on the result of the detection d_1 and hypothesis h_1 (LO setting), the receiver calculates *a posteriori* Bayesian probabilities of the M possible input states of the signal: $\mathbb{B}_1 = \{\zeta_1(1),\zeta_1(2),\ldots,\zeta_1(m),\ldots,\zeta_1(M)\}$. The receiver chooses the most likely state of the incident signal based on the Bayesian probabilities, i.e., the one with the maximum *a posteriori* probability. This result becomes the new hypothesis and is fed forward to the next stage, where the LO setting is prepared to null this new hypothesis. The *a posteriori* probabilities for stage k, B_k, thus correspond to the *a priori* probabilities for stage $k+1$. This procedure is repeated for each successive stage, gaining more certainty about the state of the signal. At each discrimination stage the hypothesis is based on the history of all the former stages' measurements and the decision is made using Bayes' rule:

$$\zeta_k(m|d_k,\langle n_k(m,h_k)\rangle) = \frac{P(d_k|\langle n_k(m,h_k)\rangle)\zeta_{k-1}(m)}{\sum_{j=1}^{M}P(d_k|\langle n_k(j,h_k)\rangle)\zeta_{k-1}(j)}, \quad (5)$$

where $P(d_k|\langle n_k(m,h_k)\rangle)$ is the probability of the detection result d_k at stage k, given that the symbol m was sent, the LO was set to test the symbol hypothesis h_k, and the photon mean number of the total field at stage k is $\langle n_k(m,h_k)\rangle$. $\zeta_k(m)$ becomes the *a priori* probability of the possible symbol m before measurement at stage $k+1$, and this probability depends on the history of the detections and hypotheses of the previous $k-1$ SD stages and on the *a priori* probabilities $\mathbb{B}_0$:

$$\zeta_k(m) = \sum_{\mathbb{D}_k}\sum_{\mathbb{H}_k}\zeta_k(m|\mathbb{D}_k,\mathbb{H}_k,\mathbb{B}_0)P(\mathbb{D}_k,\mathbb{H}_k|\mathbb{B}_0), \quad (6)$$

where $P(\mathbb{D}_k,\mathbb{H}_k|\mathbb{B}_0)$ is the *a priori* probability of the receiver observing the set $\mathbb{D}_k = \{d_1,\ldots,d_k\}$ of detection results, and $\mathbb{H}_k = \{h_1,\ldots,h_k\}$ is the set of test hypotheses for the first k stages. We next write the probability of getting a particular detection result d_k from our detector. For a typical non-number resolving detector, d_k may take only two values, $d_k \in \{0, \neq 0\}$; while for a detector with some number-resolving capability, additional values are possible. Thus, in general, the probability of detection result d_k is

$$P(d_k|\langle n_k(m,h_k)\rangle) = \frac{\langle n_k(m,h_k)\rangle^{d_k}}{d_k!}e^{-\langle n_k(m,h_k)\rangle}, \quad (7)$$

assuming the field is coherent (i.e., Poisson statistics). However, we found little additional benefit in using number resolving detectors over binary detectors [17], thus we limit our analysis here to the performance of the receiver with binary detectors. After the final stage, $k = N$, the receiver calculates the hypothesized symbol h_{N+1} as the one with maximum *a posteriori* probability. This is the final decision of the receiver about the received state. The expected probability of error for the state discrimination of the signal is

$$P_{\rm e,SD} = 1 - \sum_{\mathbb{H}_{N+1}}\sum_{\mathbb{D}_N}\zeta_0(h_{N+1})\Gamma_0(h_1) \times\left[\prod_{j=1}^{N}P(d_j|\langle n_k(h_{N+1},h_j)\rangle)\Gamma_j(h_{j+1})\right], \quad (8)$$

where $\Gamma_k(h_j)$ selects the terms that occur in the receiver, and excludes those not allowed by the strategy $\Gamma_k(h_j) = \delta_{m_k,h_j}$ such that

$$\zeta_k(m_k|\mathbb{D}_k,\mathbb{H}_k,\mathbb{B}_0) = \max\{\zeta_k(1|\mathbb{D}_k,\mathbb{H}_k,\mathbb{B}_0),\ldots,\zeta_k(M|\mathbb{D}_k,\mathbb{H}_k,\mathbb{B}_0)\},$$

$\Gamma_0(h_1) = 1$ if $\zeta_0(h_1) = \max\{\mathbb{B}_0\}$ and zero otherwise. Sequential application of Bayes' rule gives the *a posteriori* probabilities for each symbol m at stage k in terms of the sets $\mathbb{D}_k$, $\mathbb{H}_k$, and $\mathbb{B}_0$:

$$\zeta_k(m|\mathbb{D}_k,\mathbb{H}_k,\mathbb{B}_0) = \frac{\prod_{l=1}^{k} P(d_l|\langle n(s=m,h_l)\rangle)\zeta_0(m)}{\sum_{j=0}^{M-1}\prod_{l=1}^{k} P(d_l|\langle n(s=j,h_l)\rangle)\zeta_0(j)}.$$

Calculating the probability of error from Eq. (8) can be computationally prohibitive for large numbers of stages. Therefore, the expected error rates for the receiver with more than four stages were found using Monte Carlo simulations. Figure 3 shows the error probabilities for QPSK and 8-PSK as a function of signal strength with varying numbers of stages.

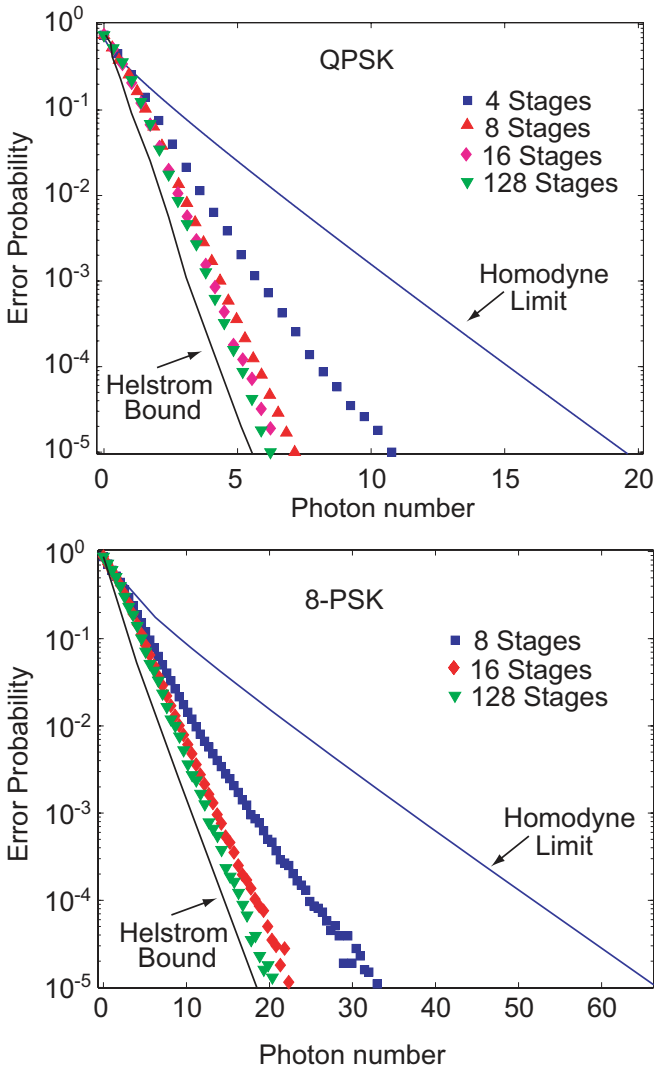

FIG. 3. (Color online) Error probability as a function of the mean number of signal photons compared to the Helstrom bound and Homodyne limit for an ideal receiver with a finite number of discrimination stages for M-ary ($M = 4$ and 8) receivers. These Monte Carlo simulations assume 100% efficient detection. The slightly nonmonotonic behavior of the simulated error probability for the case of 8-PSK at high photon number is just statistical fluctuations due to the relatively rare probability of their occurrence in our Monte Carlo simulations.

We compare the performance of the receivers to the Helstrom bound and the HL. For the equally spaced, symmetric states commonly used in M-ary PSK communication, the Helstrom bound can be well approximated using the square-root measure (SRM) [18]. The SRM for PSK signals is

$$P_{e,\mathrm{SRM}} = 1 - \frac{1}{M^2}\left(\sum_{q=1}^{M}\sqrt{\lambda_q}\right)^2, \tag{9}$$

where

$$\lambda_q = e^{-n_{\mathrm{Sig}}}\sum_{m=1}^{M}\exp\left\{(1-q)\frac{2\pi i m}{M} + n_{\mathrm{Sig}}e^{\frac{2\pi i m}{M}}\right\}$$

are eigenvalues of the Gram matrix for M-ary PSK, with the elements $G_{j,k} = \langle\psi_j|\psi_k\rangle$.

The probability of error given by the standard quantum limit (SQL) for symmetric M-ary PSK with $M > 2$ for an ideal homodyne receiver is [4]

$$P_{e,\mathrm{Hom}} = 1 - \frac{1}{\pi}\int_{-\frac{\pi}{M}}^{\frac{\pi}{M}}\int_{0}^{\infty} e^{-|r\exp(i\theta)-\sqrt{n_{\mathrm{Sig}}}|^2} r\,dr\,d\theta. \tag{10}$$

Figure 3 shows that this strategy surpasses the performance of homodyne receivers and approaches the ideal error probability as defined by the Helstrom bound as the number of discrimination stages increases.

We apply this strategy to experimentally investigate receivers for QPSK signals by emulating the feed-forward process to update the LO phase for each discrimination stage. We do this emulation for receivers with four and eight discrimination stages. Receivers using this strategy can surpass the HL with a moderate number of discrimination stages and efficiencies achievable with off-the-shelf detectors and optical components.

III. EXPERIMENTAL INVESTIGATION OF A RECEIVER FOR QPSK SIGNALS USING POSTPROCESSING

The QPSK modulation scheme encodes information in four possible phases of the signal $|\alpha\rangle$, $\{0,\pi/2,\pi,3\pi/2\}$, producing a four-element alphabet $\{|\alpha\rangle,|i\alpha\rangle,|-\alpha\rangle,|-i\alpha\rangle\}$ as shown in the inset of Fig. 4. We describe the experimental investigation of a receiver for QPSK signals emulating a feed-forward process and multiple discrimination stages with the goal of reaching error probabilities below the HL.

Figure 4 shows the experimental configuration for the four-stage emulator of a receiver for QPSK signals. A frequency-stabilized helium-neon laser with a linewidth $\approx$200 kHz passes through an acousto-optic modulator (AOM). A single-mode fiber (SMF) collects the first-order beam from the AOM and directs it to the optical setup of the experiment. A field programable gate array (FPGA) modulates the input power of the AOM, producing optical pulses 100 ns long at a rate of 11 kHz with rise and fall times of 20 ns. After the SMF the on-off extinction ratio of the light pulse is $\approx 10^6$. A photodiode (PD) collects a small portion of the light for intensity stabilization using feedback to the AOM. The average power is stable to better than 0.1% (peak-to-peak) in both continuous wave (cw)

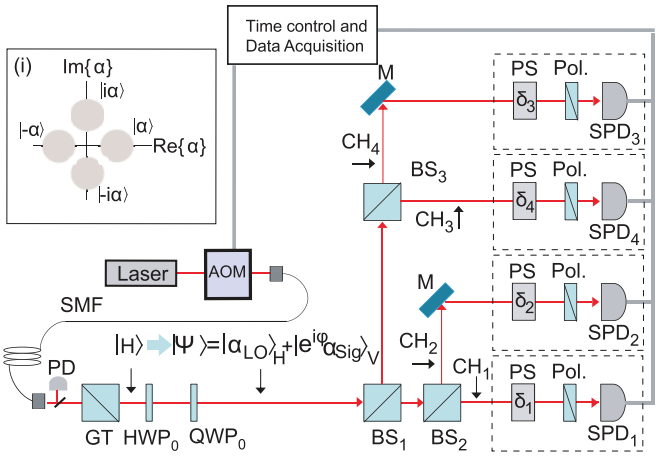

FIG. 4. (Color online) Experimental configuration for emulating a QPSK receiver. An acousto-optic modulator (AOM) prepares light pulses at 633 nm, and a high extinction-ratio polarizer (GT) defines the input horizontal polarization (H) after a single-mode fiber (SMF). A half wave plate (HWP_0) and a quarter wave plate (QWP_0) prepare the signal $|e^{i\phi}\alpha_{\rm Sig}\rangle_{\rm V}$ and the local oscillator $|\alpha_{\rm LO}\rangle_{\rm H}$ with V and H polarization, respectively, with a given relative phase and intensity resulting in a total field $|\Psi\rangle$. Three 50:50 beam splitters (BS_i) split the signal and LO in four beams that are directed to analyzer stages consisting of phase shifters (PS) and polarizers. Single-photon detectors (SPD_i) detect the total field in each stage for specific induced phase shifts δ_i and the results are saved for postprocessing. Inset (i) shows the possible states for the QPSK signal $|e^{-i\phi}\alpha\rangle$, $\phi = \{0,\pi/2,\pi,3\pi/2\}$.

and pulsed modes. A high extinction-ratio polarizer transmits horizontal polarization (H) and defines the LO polarization with an extinction ratio better than 10^5.

We generate the signal and LO from one beam with specific relative phase shifts. A slight rotation of the half wave plate HWP_0 generates the signal (Sig) in the orthogonal (vertical) polarization mode with respect to the LO with a signal-to-LO intensity ratio of 1:100. This defines the entry point of the signal into the receiver in analogy to the receiver in Fig. 1, where the signal is combined with the LO with orthogonal polarization using a polarizing beam splitter (PBS). We use the combination of the HWP_0 and a quarter wave plate (QWP_0), rotated at specific angles by motorized rotation stages, to generate the four phase states of the signal with respect to the LO: $\phi = \{0,\pi/2,\pi,3\pi/2\}$. We pay special attention on the calibration of the wave-plate rotation angles when using SPDs to prevent damage to the SPDs from excessive light levels that could result from unintended rotations of a wave plate. The copropagating signal and LO are split into four paths using three 50:50 beam splitters (BS_i) with each beam entering a discrimination stage. The fields of each of these beams are now described by Eq. (1) with four possible values for the phase ϕ.

The analyzer stages consist of a quartz plate with its optical axis along the vertical, used as a variable phase shifter (PS), and a polarizer consisting of a half wave plate (HWP) and a PBS. These components are arranged to null a particular signal input phase, i.e., to generate destructive interference at the output of the polarizer.

The phase shifter adds an extra phase shift between the signal and LO through the quartz plate's birefringence. A tilt of the quartz plate (rotation around a vertical axis perpendicular to the propagation direction) changes the relative optical paths of the signal and LO. We use this phase shift to null the signal with respect to the LO. The relative phase shift, δ, as a function of the quartz-plate tilt angle θ is given by [19]

$$\delta = \frac{2\pi\,\Delta n}{\lambda} d\left(\cos\left\{\arcsin\left[\frac{\rm n_{air}}{\rm n_1}\sin(\theta)\right]\right\}\right)^{-1}, \qquad (11)$$

where $\Delta n = n_e - n_o = 0.0091$ is the difference of the index of refaction of the ordinary (o) and extraordinary (e) rays at $\lambda = 633$ nm, $d = 1$ mm is the quartz plate thickness, $n_{\rm air} \approx 1$ is the index of refraction of light in air, and $n_1 \approx 1.455$ is the average of the e and o indices of refraction in quartz [20]. The state of the total field in a given stage after the PS is given by Eq. (2) with the extra phase shift defined by Eq. (11). The relative phase of the signal and the LO is now $\phi - \delta + \pi$, and this state is projected onto the signal polarization at the output of the polarizer (see Fig. 4).

Figure 5 shows the relative intensity of the mixed signal and LO (for four input phases of the signal), as projected by the polarizer and measured by a photodiode, for a particular stage versus the quartz-plate tilt angle. The functional form is given by Eq. (4) together with Eq. (11). For these measurements we use a strong cw input, of ≈0.5 mW, and motorized control of the quartz-plate tilt angles. For a given phase of the prepared input state ϕ relative to the LO, there is a quartz-plate tilt angle β that nulls the signal with the LO. We define this angle as the nulling angle for a given signal phase. The minimum-to-maximum intensity ratio in the interference fringes is $\approx 5 \times 10^{-3}$ (see Fig. 5), which is consistent with the 1×10^4 extinction ratio at the LO polarization of the PBS in the discrimination stages (polarizers in Fig. 4) along with the 1×10^{-2} signal-to-LO intensity ratio. We note that this results in an expected constant background of ≈1% in the projected intensity.

We use a detector [21] calibrated with a 0.05% 1σ uncertainty and a series of optical attenuators to measure the absolute radiant power of the light. This detector allows us to measure the signal's average photon number per pulse with an uncertainty below 1%. This uncertainty is dominated mainly by the calibration uncertainty of the attenuators that prepare the signal at the single-photon level. We use the same method to measure the detection efficiency of the single-photon detector used in our experiment. We detect the mixed signal and LO after the polarizer using a commercially available photocounting module SPD with a 2 nm bandpass filter at 633 nm and an antireflection coated lens. The measured DE for the filter-lens-detector assembly is 82(2)%[1] at 633 nm with a dark count rate of 100 counts per second. Since we had only a single SPD at this efficiency, we implemented Fig. 4 by looking at each channel separately and directing that channel's output to the single SPD. In our experiment we did treat each placement of the SPD as a unique detector and measured its

[1]All uncertainties quoted in this paper represent 1 standard deviation, combined statistical and systematic uncertainties.

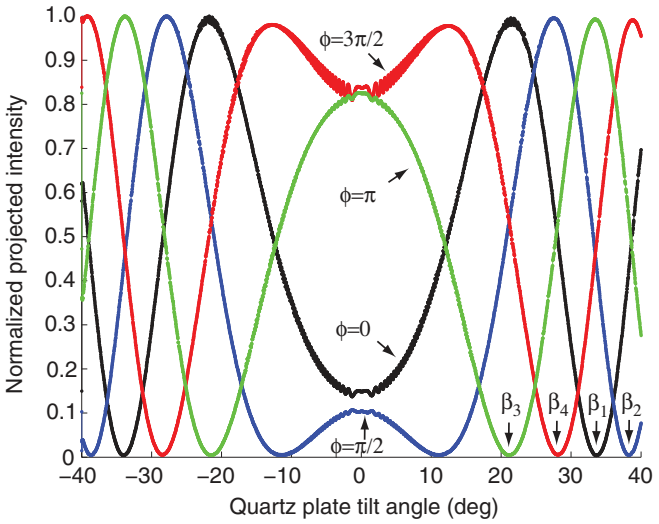

FIG. 5. (Color online) Measured projected intensity of the field containing the signal and LO for four relative phase shifts, $\phi = \{0,\pi/2,\pi,3\pi/2\}$, as a function of tilt angle of the quartz plate around the vertical axis perpendicular to the light propagation direction. The projected intensity shows destructive interference (signal nulling) at specific quartz-plate tilt angles $\{\beta_1,\beta_2,\beta_3,\beta_4\}$ for the input phase states $\phi = \{0, \pi/2,\pi, 3\pi/2\}$, respectively.

DE *in situ*, thus we henceforth refer to each placement as a unique SPD.

The FPGA provides the clock for the experiment at 11.7 kHz and records the number of detections registered by the SPDs during the photon pulse for postprocessing. A computer controls the tilt angles of the quartz plates. This defines the settings for different combinations of nulling angles β_i. The computer also collects the SPD detections for a given number of trials, input signal states, and average signal photon number per pulse for all possible LO settings.

It is possible to analyze the collected data as the four-stage discrimination receiver shown in Fig. 4, with different DEs in each stage reflecting the variation in losses in our implementation (see the Appendix). (In this case there is a direct correspondence between the SD stages in Fig. 1 and the four stages in Fig. 4.) However, it is also possible (and more convenient) to analyze the collected data to investigate different multiple-stage receivers, for which the total system DE is a fixed number. These scenarios are constructed from the data collected from a particular discrimination stage, with a fixed DE, so that the multiple-stage receivers we emulate consist of multiple replicas of the same stage. This emulation, built using data sets from single discrimination stages of Fig. 4 to create the receiver strategy of Fig. 1, allows us to study the dependence of receiver performance on the number of stages and system losses, as well as to compare our results with the theoretical model.

IV. ANALYSIS AND RESULTS

We analyze the collected data to study the specific scenarios of receivers with four and eight stages and different total system DEs. In the case of eight-stage receivers, the data are evaluated for higher photon numbers, since the power of the signal entering the receiver would have to be two times higher than that of a four-stage receiver to distribute the same amount of energy in each stage. We apply the discrimination strategy described in Sec. II for the case of QPSK signals.

Because the receiver strategy requires actual event probabilities, we use the experimentally determined probabilities $P_{\exp}(d_k|n_k(m,h_k))$ obtained from the collected data instead of the ideal probabilities from Eq. (7); this includes the effects of all system characteristics such as system detection efficiency, detector dark counts, fringe visibility, etc. [17]. These probabilities are calculated from the measurement results of all the combinations of signal phase and LO phase (SD hypothesis).

As mentioned above, we use the collected data from a single SD stage of using the SPDs as shown in Fig. 4 to construct the emulated receiver via postprocessing. We do this for each emulated scenario by separately taking the data from each of the four SDs of Fig. 4. The count rates for the SPDs depend on the relative signal and LO phases and the signal average photon number. For a signal average photon number of 1, the typical count rates for the four relative signal and LO phases $\{\pi, 3\pi/2,0, \pi/2\}$ are {25, 3100,6600, 3100} per second, respectively, and these rates increase for higher photon numbers. The effect of detector dark counts is negligible since we collect data only when the light pulse is expected at the detectors. The receiver emulation assigns a random hypothesis for the signal to be tested in the first stage and uses the result of a single measurement chosen from the collected data set for this hypothesis (LO setting). Based on the result, it determines *a posteriori* probabilities for the possible input states of the signal using Eq. (5) and the experimental probabilities $P_{\exp}$ (the $P_{\exp}$ *a priori* probabilities are assumed equal for the first SD stage), and determines the most likely signal being received. This most likely signal becomes the new hypothesis to test in the next SD stage and a new measurement is made. From this new result, updated *a posteriori* probabilities are calculated using Eq. (5). This emulation procedure is repeated as many times as the number of stages in the emulated receiver. (Note that each data point is used only once in this emulation.) At the end, the most likely state for the signal is the final maximum *a posteriori* probability of the receiver. If this final guess is the same as the real input signal, it is counted as a success; otherwise, it is counted as an error. The probability of error is equal to the number of errors divided by the number of trials (4×10^4). We experimentally investigate the error probabilities for signals with many different average photon numbers.

Different scenarios were emulated for a range of total system DEs representing the actual losses found in the different analyzer channels in our setup (CH_i in Fig. 4 accounting for losses in the optical components and detection efficiencies). The difference in losses includes not just transmittance losses, but also imperfect splitting and polarizer extinction ratios. The DE of the SPD as measured in each stage is the same to within the experimental uncertainty: $DE_{SPD} = 82(2)\%$. The total system DE for each stage, which can be seen in the last row of Table II of the Appendix, is the product of the total transmittance for each stage and the estimated DE of the SPD in the channel.

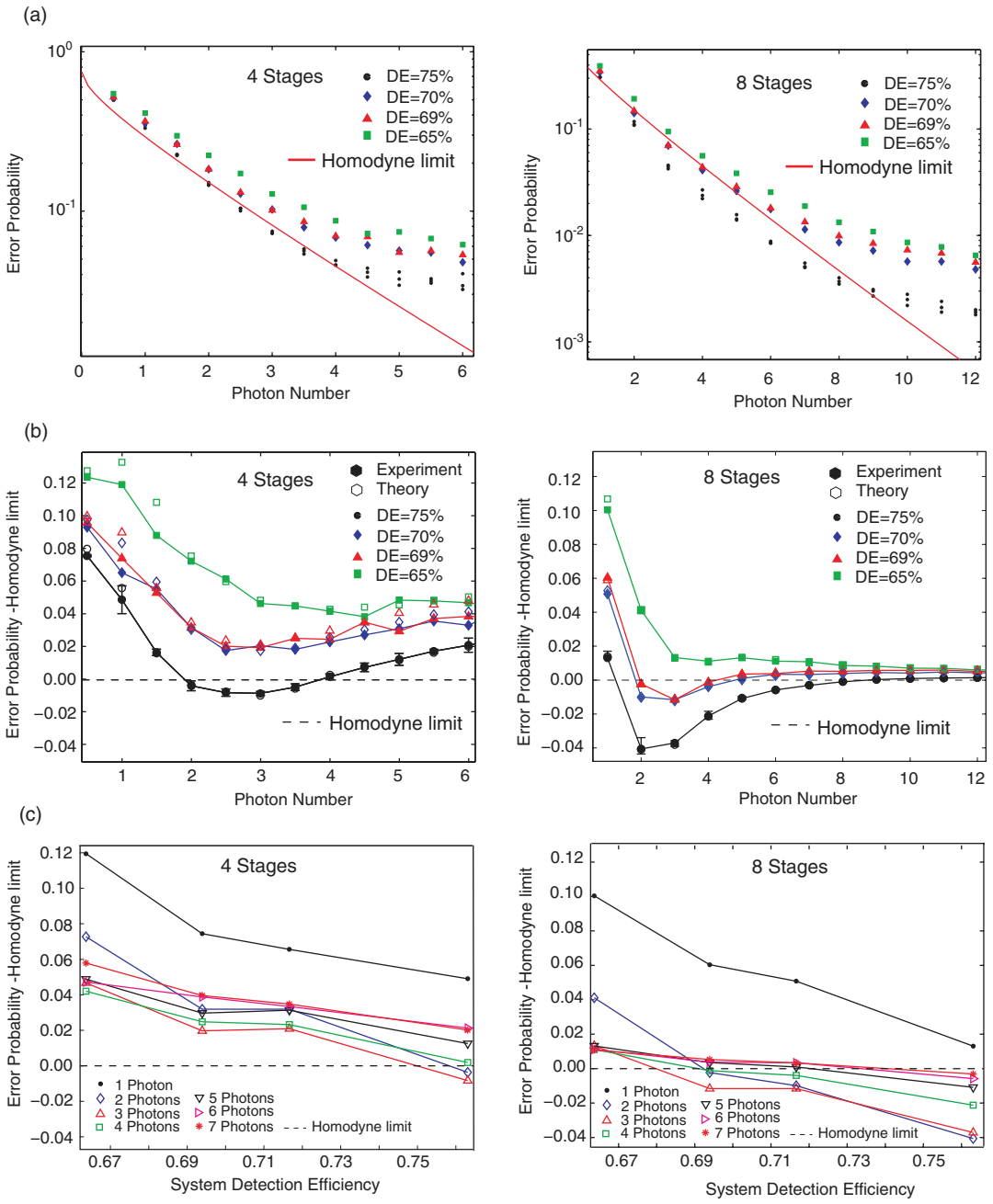

FIG. 6. (Color online) (a) Error probabilities as a function of photon number for receivers composed of four and eight identical-DE SD stages. Four such receiver systems are shown, each with a different DE as indicated (filled markers), along with the homodyne limit (red solid line). (b) Error probabilities with the homodyne limit subtracted (filled markers), together with the theoretical predictions made using the experimental probabilities (open markers). Dashed line at 0 corresponds to the homodyne limit. In (a) and (b) three sets of measurements were made for the scenario with DE = 75% to see the variation of the results. The error bars in (b) represent 1σ statistical uncertainty, although some are too small to be seen. Theory points are plotted for all measurements in (b) but many theory points are hidden by the data points. (c) Error probabilities with the homodyne limit subtracted (dashed line) as a function of photon number, from 1 to 7, vs system DE of four-stage and eight-stage receivers. Note that the eight-stage receivers outperform the four-stages receivers for all system DEs. Solid lines in (b) and (c) are guides for the eye.

Figure 6(a) shows the error probability for receivers with four equal-DE stages (left) and eight equal-DE stages (right) for different total DEs, together with the homodyne limit for QPSK signals (solid lines). Different scenarios are emulated using data collected from different analyzer channels CH_i of Fig. 4 with the measured DEs. Also seen is a test of overall variation made by repeating three runs of the experiment for the scenario with all stage DE's equal to 75%. Note that the different photon-number range in the horizontal axis of the eight-stage scenarios is double the range used for the four-stage scenarios.

TABLE I. Estimated transmittance of individual 50:50 beam-splitter transmission (T) and rejection (R) ports. .

BS	T	R
BS_1	50.4(5)%	47.0(3)%
BS_2	49.4(2)%	46.3(3)%
BS_3	48.9(3)%	47.1(4)%

Figure 6(b) shows the differences between the measured error probability and the homodyne limit for the four- and eight-stage scenarios. The four-stage scenario with a system DE = 75% shows error probabilities below the HL for signals with average photon numbers of 2 to 3.5, while the eight-stage scenario for the same DE achieves error probabilities below this limit for signals covering a wider range with average photon numbers of 2 to 8 and goes below the HL to a much greater degree. The theoretical predictions (open circles) are the result of a Monte Carlo simulation with 4×10^5 trials based on the strategy described in Sec. II. This simulation used the experimentally determined probabilities for both the discrimination Bayesian strategy and the generation of the random data. This use of experimentally determined probabilities is validated by the excellent agreement between the experimental results and the theoretical predictions. These analysis results demonstrate that the receiver strategy proposed can achieve error probabilities significantly below the HL for QPSK, and that more discrimination stages allow error probabilities farther below that limit and for a wider range of photon numbers.

The error probability as a function of DE, as shown in Fig. 6(c), highlights the improved performance of the receivers with increasing system DE from 65% to 75% for a given photon number, and the improvement of eight-stage receivers over one with four stages (with similar system DEs).

V. CONCLUSION

We described a strategy for state discrimination of nonorthogonal M-ary phase states with error probabilities below the homodyne limit. This strategy uses feed forward to update a reference local oscillator for signal nulling in multiple discrimination stages. This allows error probabilities that approach the corresponding Helstrom bounds for a moderate number of discrimination stages for signals in QPSK and 8-PSK formats. We experimentally apply this strategy to study the state discrimination for four nonorthogonal symmetric states (QPSK signals) using postprocessing to emulate the feed-forward process and multiple discrimination stages. We analyze scenarios of receivers with four and eight discrimination stages with different total detection efficiencies, and observe error probabilities below the homodyne limit. As this system used off-the-shelf components and detectors, this analysis demonstrates the feasibility for M-ary-state discrimination below the HL using feed forward with a small number of discrimination stages and moderate detection efficiencies. We do note that while performance below the HL is shown to be feasible, the scalability of this scheme to allow performance approaching the Helstrom bound is still to be determined.

ACKNOWLEDGMENTS

The authors thank Nick Bertone for the loan of the single-photon-counting module.

APPENDIX: LOSSES FROM OPTICAL COMPONENTS

The performance of state discrimination receivers depends on the efficiency with which the signal to be discriminated is detected. This efficiency is the total system detection efficiency including the SPD DE and the total transmittance of the optical components in the receiver.

Table I shows the transmittance of the individual BSs used in the experiment (see Fig 4). Table II shows the estimated transmittances of the individual optical components and the total transmittances for different discrimination stages. Note the difference in total transmittance is due mainly to the 50:50 BSs. The total detection efficiency as seen in the last row of Table II is the product of the total transmittance for each stage and the estimated DE of the SPD.

TABLE II. Estimated signal transmittance of the optical components, total transmittance, and total DE for each discrimination stage. The total DE is calculated from the total stage transmittance and the measured SPD DE: $DE_{SPD} = 82(2)\%$

	Stage			
Component	1	2	3	4
BS ports	$BS_1(T)BS_2(T)$	$BS_1(T)BS_2(R)$	$BS_1(R)BS_3(T)$	$BS_1(R)BS_3(R)$
(BSs trans.)/25%	99.6(4)%	99.3(2)%	91.2(3)%	88.5(3)%
Quartz plate	97.1(2)%	99.1(2)%	98.0(2)%	98.0(2)%
HWP	96.7(2)%	96.8(2)%	96.3(2)%	95.0(2)%
PBS projection	98.5(2)%	96.7(2)%	97.7(2)%	97.0(2)%
Total transmittance	92.1(6)%	86.6(6)%	84.7(6)%	80.0(6)%
SPD DE	82(2)%	82(2)%	82(2)%	82(2)%
Total DE	75(2)%	71(2)%	69(2)%	65(2)%

[1] C. W. Helstrom, *Quantum Detection and Estimation Theory, Mathematics in Science and Engineering*, Vol. 123 (Academic, New York, 1976).

[2] C. H. Bennet and G. Brassard, in *Proceedings of the IEEE International Conference on Computers, Systems, and Signal Processing, 1984* (IEEE, New York, 1984), p. 175.

[3] B. Huttner, N. Imoto, N. Gisin, and T. Mor, Phys. Rev. A **51**, 1863 (1995).

[4] J. G. Proakis, *Digital Communications,* 4th ed. (McGraw-Hill, New York, 2000).

[5] G. D. S Betti and E. Lannone, *Coherent Optical Communications Systems* (Wiley, New York, 2000).

[6] V. Giovannetti, S. Guha, S. Lloyd, L. Maccone, J. H. Shapiro, and H. P. Yuen, Phys. Rev. Lett. **92**, 027902 (2004).

[7] R. S. Bondurant, Opt. Lett. **18**, 1896 (1993).

[8] M. Usuga, C. Muller, C. Wittmann, M. Takeoka, U. Andersen, and G. Leuchs, in *Lasers and Electro-Optics* 2009 *and the European Quantum Electronics Conference. CLEO Europe - EQEC* 2009, [http://www.opticsinfobase.org/].

[9] R. S. Kennedy, Research Laboratory of Electronics, MIT, Technical Report No. 110, 1972 (unpublished).

[10] S. J. Dolinar, Research Laboratory of Electronics, MIT, Quarterly Progress Report No. 111, 1973 (unpublished).

[11] M. Takeoka, M. Sasaki, P. van Loock, and N. Lütkenhaus, Phys. Rev. A **71**, 022318 (2005).

[12] M. Takeoka and M. Sasaki, Phys. Rev. A **78**, 022320 (2008).

[13] R. L. Cook, P. J. Martin, and J. M. Geremia, Nature **446**, 774 (2007).

[14] C. Wittmann, M. Takeoka, K. N. Cassemiro, M. Sasaki, G. Leuchs, and U. L. Andersen, Phys. Rev. Lett. **101**, 210501 (2008).

[15] K. Tsujino, D. Fukuda, G. Fujii, S. Inoue, M. Fujiwara, M. Takeoka, and M. Sasaki, Opt. Express **18**, 8107 (2010).

[16] K. Tsujino, D. Fukuda, G. Fujii, S. Inoue, M. Fujiwara, M. Takeoka, and M. Sasaki, Phys. Rev. Lett. **106**, 250503 (2011).

[17] J. T. Kosloski, G. B. Baumgartner, and J. Goldhar (to be published).

[18] K. Kato, M. Osaki, M. Sasaki, and O. Hirota, IEEE Trans. Comm. **47**, 248 (1999).

[19] B. E. A. Saleh and M. C. Teich, *Fundamentals of Photonics* (Wiley, New York, 2007).

[20] E. D. Palik, *Handbook of Optical Constants of Solids* (Academic, New York, 1989).

[21] T. R. Gentile, J. M. Houston, and C. L. Cromer, Appl. Opt. **35**, 4392 (1996).